AIAA AVIATION Forum
June 25-29, 2018, Atlanta, Georgia
2018 AIAA/CEAS Aeroacoustics Conference

10.2514/6.2018-3143

Application of Amiet's theory for noise prediction of general airfoil profiles subjected to spanwise-varying inflow conditions

Renato Fuzaro Miotto * William Roberto Wolf †
University of Campinas, Campinas, SP, 13083-860, Brazil

Leandro Dantas de Santana ‡ Cornelis H. Venner §
University of Twente, Drienerlolaan 5, 7522 NB, Netherlands

In this paper, three different techniques are combined to provide a complete physics-based semi-anytical model for leading-edge noise prediction. The model is based on the classical theory of Amiet. Here, the two-dimensional turbulence spectrum is computed by a model based on the rapid distortion theory and the aeroacoustic transfer function is numerically evaluated by the boundary element method to account for the effects of the general airfoil profiles. The influence of spanwise inhomogeneities is also considered through the application of the inverse strip method. An assessment of each individual technique on the radiated noise is provided. This research shows that the turbulence distortion occurring at the leading-edge plays a significant role on the predicted noise levels. Compared with the von Kármán model for isotropic turbulence, the rapid distortion theory predicts reduced noise levels at high-frequencies and increased levels at low-frequencies. This paper also shows that the spanwise-varying inflow, here represented by a linearly varying condition, contributes to raising the acoustic radiation when compared to the similar uniform inflow case. By considering modifications on the airfoil leading-edge radius and on the airfoil overall thickness, we show that the leading-edge bluntness plays a key role on reducing gust-airfoil interaction noise. This observation is more pronounced for microphones positioned downstream of the airfoil and for high frequencies.

Introduction

Turbulence-airfoil interaction is a major source of broadband noise generated by rotating blades such as those found in fans, wind turbines, contra-rotating open rotors and helicopters [1–5] . With the more stringent noise regulations, it is necessary to improve our understanding of the noise generation mechanisms to mitigate them. A promising strategy consists in directly modify the blade shapes to reduce their acoustic response to the incoming flow. Recent studies show that the modification of the airfoil shape [4, 6], the application of leading-edge serrations and other wavy shapes [7–9] and, also, porosity [10] may drastically alter the acoustic field radiated by turbulence impinging on a leading edge.

In order to understand the effects of the leading-edge geometry on the radiated noise, it is important to develop techniques for its prediction. There are still several difficulties in accurately predicting leading-edge noise due to the wide range of temporal and spatial scales involved on its generation. Direct numerical simulation, DNS, and experimental methods are powerful techniques that allow the study of both the noise generation mechanisms and their propagation. However, such methodologies have inherent costs associated with large-scale time-consuming computations and aeroacoustic wind tunnel facilities.

Semi-analytical and semi-empirical models are associated with lower costs than the previously described methodologies. However, they usually have simplifications which may impact their accuracy for design/optimization applications. A well-known semi-analytical model for leading-edge noise prediction by an incident turbulent gust was provided by Amiet [11]. This methodology considers a thin airfoil immersed in a homogeneous isotropic turbulent stream convected through a uniform mean flow under Taylor's hypothesis of frozen turbulence. In this classical theory, the power spectral density (PSD) of the acoustic pressure is related to the farfield sound through Curle's analogy [12]. The latter prescribes that the noise radiated by a solid body immersed in a turbulent stream is related to its surface pressure fluctuations.

*Graduate student, Department of Energy, AIAA member.
†Assistant Professor, Department of Energy, AIAA Member.
‡Assistant Professor, Faculty of Engineering Technology, Department of Engineering Fluid Dynamics, AIAA Member.
§Professor, Faculty of Engineering Technology, Department of Engineering Fluid Dynamics, AIAA Member.

Howe's theory of vortex sound [13] also provides an explanation for turbulence-airfoil interaction noise, where the unsteady surface pressure distribution in the proximity of the airfoil leading edge is proportional to the dipole sources induced by the vortex generated velocity field.

The unsteady pressure distribution over the airfoil surface can be determined using the two-dimensional incompressible theories of Kussner [14] and Sears [15], who considered a distribution of vortex singularities over the airfoil and wake to conserve the vorticity in the entire field. Such linearized approximation was extended to include some additional effects such as three-dimensionality, airfoil camber, angle of attack and blade thickness [16–18] . Recently, Ayton and Peake [19] proposed a theoretical model for a weakly non-parallel shear flow at high frequencies and low Mach numbers over an airfoil with small thickness using the principle of matched asymptotic expansions and the rapid distortion theory (RDT).

Numerical methodologies have also been proposed to account for complex incident flows and realistic airfoil geometries [20–22] . Glegg and Devenport [23] adopted a panel method to predict turbulence-airfoil interaction noise, obtaining good agreement with Amiet's theory at low frequencies, where the airfoil unsteady lift response is computed based on Sears' method. Recently, Miotto *et al.* [24] developed a boundary element method (BEM) to determine the lift response of an airfoil of arbitrary shape due to incident supercritical compressible gusts, being suitable for high-frequency regimes where compressibility effects become important.

In the present paper, we combine the aforementioned BEM approach with the inverse strip method presented by Christophe *et al.* [25] to predict the airfoil leading-edge noise with effects of spanwise-varying inflow conditions. The modification of the von Kármán spectrum based on the rapid distortion theory, as proposed in Ref [26], is also employed. Here, the contribution of each of these techniques on the far-field noise prediction by gust-leading-edge interaction is investigated.

Theoretical background

Acoustic radiation - Amiet's theory

Let us consider an airfoil of span $2d$ and chord $2b$ ($d \gg b$ or $k\,d \gg 1$) located in a Cartesian coordinate system with origin at the airfoil mid-chord and mid-span. The airfoil is subject to a gust represented by the wall-normal velocity component $w = w_0 \exp\{\mathrm{i}\,[k_1(U_0 t - x) - k_2 y]\}$. Following this notation, Amiet [11] proposed an expression for the radiated acoustic pressure PSD as follows

$$S_{pp}(\mathbf{x}, \omega) = \left(\frac{\rho_0\, k\, z\, b}{r_o^2}\right)^2 \pi\, U_0\, d\, \Phi_{ww}(k_1, k_2)\, |\mathcal{L}(\mathbf{x}, k_1, k_2)|^2 \,. \tag{1}$$

In the equation above, $\mathbf{x} = (x, y, z)$ is the observer position, ω is the frequency, k_1 and k_2 are the x and y direction hydrodynamic wavenumbers, respectively. The term $r_o = \sqrt{x^2 + \beta^2(y^2 + z^2)}$ represents the observer position corrected for convective effects, where $\beta = \sqrt{1 - M_0^2}$ is the compressibility factor. The observer positions x, y, z are measured, respectively, in the chordwise, spanwise and wall-normal Cartesian directions. The incoming gust amplitude is w_0, and the freestream velocity, Mach number and density are U_0, M_0 and ρ_0, respectively, and k is the acoustic wavenumber.

The term $\mathcal{L}$ is the effective lift function per unit span including retarded time effects, also known as aeroacoustic transfer function. It can be analytically determined for a flat plate [27] , however, noteworthy differences are observed for thick airfoil profiles since the magnitude of the unsteady pressure distribution along the airfoil surface is reduced [24] . Finally, Φ_{ww} stands for the inflow two-dimensional turbulence spectrum, which can be modeled by the von Kármán or Liepmann spectrum for isotropic turbulence [28] . When the airfoil thickness is no longer negligible, a model for Φ_{ww} can be derived based on the rapid distortion of turbulence along the leading edge [26] .

Aeroacoustic transfer function for general airfoil profiles

The aeroacoustic transfer function is defined by Amiet for an infinitely thin plate as [11]

$$\mathcal{L}(\mathbf{x}, k_1, k_2) \quad = \quad \int_0^2 g(x_s, k_1, k_2)\, \exp[-\mathrm{i}kb(x_s - 1)(M_0 - x/r_o)/\beta^2]\mathrm{d}x_s \,, \tag{2}$$

where x_s is a particular dipole source position along the airfoil chord. Here, $g(x_s, k_1, k_2)$ is the transfer function that relates the airfoil unsteady pressure jump (represented by $\Delta p = p^{lower} - p^{upper}$) to the incident gust of amplitude w_0,

and that is given by [11]

$$g(x_s, k_1, k_2) = \frac{\Delta p(x_s, y_s, t)\ \exp[\,\mathrm{i}(k_2 y - \omega t)]}{2\,\pi\,\rho_0\,U_0\,w_0}\,. \tag{3}$$

In order to compute the aeroacoustic transfer function for general airfoil profiles, we will describe a theoretical methodology that can be solved numerically by the BEM. Starting from the boundary value problem prescribed by the linearized airfoil theory, one can write a canonical Helmholtz equation in the transformed Prandtl-Glauert plane as

$$\phi'_{\bar{x}\bar{x}} + \phi'_{\bar{z}\bar{z}} + K^2\phi' = 0\,, \quad \text{where} \quad K^2 = \frac{b^2}{\beta^2}\left(\frac{k^2}{\beta^2} - k_2^2\right) \tag{4}$$

$$\phi'(\bar{x}, 0) = 0 \qquad , \quad \bar{x} \le 0 \tag{5}$$

$$\phi'_{\bar{z}}(\bar{x}, 0) = -\frac{w_0 b}{\beta}\,\exp\left(-\frac{\mathrm{i}k_1 b\bar{x}}{\beta^2}\right) \qquad , \quad 0 < \bar{x} < 2 \tag{6}$$

$$\phi'_{\bar{x}} + \frac{\mathrm{i}k_1 b}{\beta^2}\phi' = 0 \qquad , \quad \bar{x} \ge 2\,. \tag{7}$$

This set of equations represents the perturbation potential along an airfoil immersed in a turbulent gust. The boundary conditions of the problem are given by the Sommerfeld radiation condition upstream the leading edge of the airfoil, the Kutta condition along the airfoil wake and the no penetration condition along the solid airfoil surface. Here, $\phi' = \phi'(x, z)$ is a gust complex amplitude. It is worth mentioning that, at this stage, the origin of the coordinate system is shifted to the airfoil leading edge and the non-dimensional airfoil chord is $2b = 1$. This boundary value problem is obtained after the non-dimensionalization of the convective wave equation, such that

$$\bar{x} = \frac{x}{b}, \qquad \bar{y} = \frac{\beta y}{b}, \qquad \bar{z} = \frac{\beta z}{b}\,.$$

The BEM approach proposed in Ref. [24] allows the calculation of the aeroacoustic transfer function for general airfoil profiles. The proposed approach numerically solves the boundary value problem prescribed by the linearized airfoil theory in the transformed Prandtl-Glauert plane, providing the unsteady load distribution over the airfoil surface. This methodology considers the iterative application of the BEM calculation in an approach equivalent to consequent Schwarzschild solutions. Here, we apply the boundary conditions satisfying both the semi-infinite leading-edge noise problem due to an impinging gust and its subsequent semi-infinite airfoil with the trailing-edge scattering effect. This method is valid for blades of large aspect ratios subjected to three-dimensional supercritical perturbations and compressible subsonic inflows.

Initially, we assume a zeroth-order potential solution $\phi'^{(0)}$ which satisfies the non-penetration boundary condition through the plane $\bar{z} = 0$ before employing the Schwarzschild technique

$$\phi'^{(0)}(\bar{x}, \bar{z}) = -\frac{w_0}{\sqrt{k_1^2 + k_2^2}}\,\exp\left(-\frac{\mathrm{i}k_1 b\bar{x}}{\beta^2} - \frac{b\bar{z}}{\beta}\sqrt{k_1^2 + k_2^2}\right)\,. \tag{8}$$

This zeroth-order solution is then attributed to the entire (finite) computational domain. Letting S_A be part of the computational domain (namelly S) where the non-penetration boundary condition is satisfied for each iteration of Schwarzschild's technique, we define a discrete function $f_j(\mathbf{x}_s)$ such that

$$f_j(\mathbf{x}_s)\begin{cases} = 1 & \text{, if the } j\text{-th element location } \mathbf{x}_s \in S_A \\ = 0 & \text{, otherwise.} \end{cases}$$

Hence, after discretizing the surface S into J elements Γ_j, the linear system for each iteration of the Schwarzschild solution is given by

$$\left[\mathbf{H}\right]\left\{\mathbf{X}\right\} = \left[\mathbf{D}\right]\left\{\mathbf{B}\right\}\,. \tag{9}$$

Here, the coefficients of matrices $\mathbf{H}$ and $\mathbf{D}$ are named h_{ij} and d_{ij}, respectively, and are written as

$$h_{ij} = f_j\left[\delta_{ij}\,\frac{1}{2} + (1 - \delta_{ij})\int_{\Gamma_j}\frac{\partial G_{ij}}{\partial \mathbf{n}}\,\mathrm{d}\Gamma_j\right] + (f_j - 1)\left[\delta_{ij}\left(\frac{1 - \gamma - \ln(\frac{1}{4}KL_j)}{2\pi} - \frac{\mathrm{i}}{4}\right)L_j + (1 - \delta_{ij})\int_{\Gamma_j} G_{ij}\,\mathrm{d}\Gamma_j\right]$$

and

$$d_{ij} \quad = \quad (f_j - 1)\left[\delta_{ij}\,\frac{1}{2} + (1-\delta_{ij})\int\limits_{\Gamma_j}\frac{\partial G_{ij}}{\partial \mathbf{n}}\,\mathrm{d}\Gamma_j\right] + f_j\left[\delta_{ij}\left(\frac{1-\gamma-\ln(\frac{1}{4}KL_j)}{2\pi} - \frac{\mathrm{i}}{4}\right)L_j + (1-\delta_{ij})\int\limits_{\Gamma_j} G_{ij}\,\mathrm{d}\Gamma_j\right],$$

where δ_{ij} is the Kronecker delta, γ is the Euler-Mascheroni constant ($\gamma = 0.5772156649...$) and L_j is the length of panel Γ_j. The integrals over each panel Γ_j are numerically computed using Gaussian quadrature.

In the equations above, the normal derivative points inward to the surface and the frequency domain two-dimensional Green's function is defined as

$$G(\mathbf{x}|\mathbf{x}_s) \equiv -\frac{\mathrm{i}}{4}H_0^{(2)}(K||\mathbf{x}-\mathbf{x}_s||) = -\frac{\mathrm{i}}{4}H_0^{(2)}(Kr)\,. \tag{10}$$

The term $H_0^{(2)}$ is the Hankel function of zeroth-order and second type written as $H_0^{(2)} = J_0 - \mathrm{i}Y_0$, where J_0 and Y_0 are the Bessel and Neumann functions, respectively. The asymptotic behavior of the two-dimensional Hankel function as the point source $\mathbf{x}_s$ moves to the surface is already accounted for in the coefficients h_{ij} and d_{ij}. The use of the two-dimensional BEM formulation is justified since the effect of oblique gusts on the load distribution depends only on the modified wavenumber K appearing in Eq. 4.

Initially, the linear system provides the leading-edge correction $\Psi^{(1)}$ that cancels $\phi'^{(0)}$ for $\bar{x} < 0$. So that $\phi'^{(1)} = \phi'^{(0)} + \Psi^{(1)}$ represents the potential due to the semi-infinite leading-edge noise problem. In this case, the vector elements for $\mathbf{X}$ and $\mathbf{B}$, named x_i and b_i, are given by

$$x_i = f_j\,\Psi^{(1)} + (1-f_j)\,\frac{\partial \Psi^{(1)}}{\partial \mathbf{n}}\,,$$

$$b_i = (f_j - 1)\,\phi'^{(0)}\,.$$

The second iteration of the problem solves for the correction in terms of trailing-edge secondary diffraction, where the Kutta condition is satisfied

$$x_i = f_j\,\mathrm{P}^{(2)} + (1-f_j)\,\frac{\partial \mathrm{P}^{(2)}}{\partial \mathbf{n}}\,,$$

$$b_i = (f_j - 1)\,p'^{(1)}\,.$$

In this case, the result is more conveniently expressed in terms of pressure, yielding $p'^{(2)} = p'^{(1)} + \mathrm{P}^{(2)}$, where $\mathrm{P}^{(2)}$ is the variable that cancels $p'^{(2)}$ for $\bar{x} \geq 2$. This result provides an accurate evaluation of the unsteady load distribution over the airfoil surface to compute the aeroacoustic transfer function. For more details about the numerical procedure, the reader is refered to Ref. [24].

Spanwise-varying inflow conditions

The theory initially presented by Amiet [27] considers a spanwise uniform inflow. In the present work, we propose a numerical method that overcomes the challenge brought by spanwise-varying inflow conditions through the application of the inverse strip theory [25, 29]. Equation 1 assumes a large aspect ratio airfoil with a constant spanwise section subjected to a uniform flow with homogeneous turbulence. However, in most applications of engineering interest, even if the blade section is constant, the mean flow velocity and turbulence statistics are generally non-uniform.

The most straightforward approach that considers flow spanwise inhomogeneities divides the airfoil along the spanwise direction into small strips such that the total noise corresponds to the sum of contributions from each individual strip with different flow conditions [30]. When the airfoil is discretized into small strips, the infinite span hypothesis, $k\,d \to \infty$, is generally not satisfied for an individual strip and Eq. 1 does not hold. In this case, the more general formulation provided by Amiet [11] should be considered where the acoustic pressure PSD requires the integration of a cardinal sine function. The reader is referred to Refs. [25] and [11] for further details.

$$S_{pp}(\mathbf{x},\omega) = \left(\frac{\rho_0\,k\,z\,b}{r_o^2}\right)^2 \pi\,U_0\,d\int_{-\infty}^{+\infty}\frac{\sin^2\left[d\,(k_2-K_2)\right]}{\pi d\,(k_2-K_2)^2}\Phi_{ww}(k_1,k_2)\,|\mathcal{L}(\mathbf{x},k_1,k_2)|^2 dk_2\,. \tag{11}$$

Christophe *et al.* [25] demonstrate that the direct strip approach is inaccurate in the low-frequency regime and argue that if the extent of the small span strips is smaller than the spanwise correlation length of the sources, the strips are

statistically correlated and the phase variations occurring along the span can no longer be reproduced. In this case, the increasing number of strips reduces the amplitude of the calculated far field pressure PSD in the low-frequency portion of the spectrum and damps the oscillations appearing at high-frequencies.

The inverse strip theory was then proposed in [25] to overcome the theoretical limitation of the direct strip approach. In the inverse strip method, the noise produced by an airfoil strip is calculated from the subtraction of the sound computed for two large-span airfoils, with span lengths differing by the length of the short strip segment under consideration. Therefore, this approach requires two evaluations of Eq. 1 for each strip, which is computationally inexpensive and produces accurate results for low- and high-frequencies. This method is also adequate to be applied for problems with spanwise-varying inflow conditions.

Figure 1 illustrates how the inverse strip method works. The contribution from each strip $n = 1, \ldots, N$ is computed by the subtraction of the pressure PSD of a large aspect ratio (virtual) wing using the infinite span formulation (represented here by $S_{pp}^{(\infty)}$) and a second (virtual) wing at the same position but with a span length reduced by the size δ of the strip (represented by $S_{pp}^{(\infty-n)}$). Both wings have the same flow properties employed on the individual strip under consideration.

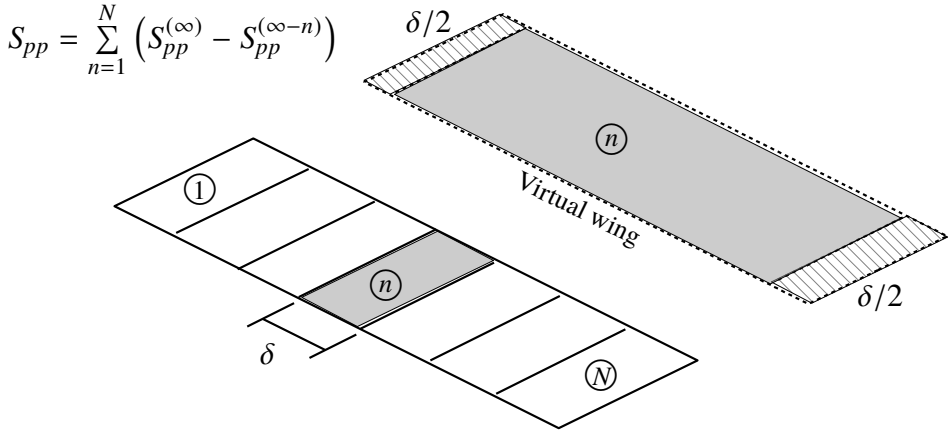

Fig. 1 Representation of the inverse strip method.

Rapid Distortion Theory

When a flat plate is considered in Amiet's theory, the von Kármán spectrum for isotropic turbulence may be employed [11] as

$$\Phi_{ww}(k_1, k_2) = \frac{4}{9\pi} \frac{u'^2}{k_e^2} \frac{k_1^2/k_e^2 + k_2^2/k_e^2}{\left(1 + k_1^2/k_e^2 + k_2^2/k_e^2\right)^{7/3}}, \tag{12}$$

where, u' stands for the RMS axial velocity fluctuations and k_e is the average wavenumber of the energy-containing eddies given by $k_e = \sqrt{\pi}\ \Gamma(5/6)/\left[\Lambda\ \Gamma(1/3)\right]$. Here, Γ is the Gamma function and Λ is the turbulence integral length scale.

Although sharp leading edges may not add considerable distortion to the turbulence, it is known that the same cannot be said for blunt leading edges. In this sense, the airfoil leading-edge bluntness induces a modification of the mean velocity field and turbulence properties [31, 32]. This phenomenon can be modeled by the rapid distortion theory when the time scale associated with the non-linear turbulent interactions is much larger than the fluid particle convection through the non-uniform flow region. The turbulence intensity should also be small enough to not significantly disturb the mean flow field. Furthermore, in the case of a turbulent flow past an airfoil leading edge, the turbulence integral correlation length scale should be larger than the boundary layer thickness [26].

The turbulence distortion occurring close to the airfoil leading edge is related to the noise reduction observed in airfoils of increasing thickness [33]. For instance, Glegg and Devenport [34] numerically predicted the high-frequency

noise reduction due to the rapid distortion of turbulence occurring in the airfoil leading-edge. Likewise, a recent study from Ayton and Chaitanya [6] based on rapid distortion theory shows, by analytical and experimental means, the effect of leading-edge radius and airfoil thickness on gust-airfoil interaction noise. For low Mach numbers, they show that blunter leading edges lead to a reduction in the far-field noise radiation. However, they also observed that at moderate Mach numbers ($M_0 = 0.6$), the blunter leading edge can increase far-field noise in the upstream direction for high-frequency gusts. This trend has been also observed in Refs. [24], [28] and [35].

Moreu *et al.* [36] proposed the modification of the turbulence upwash velocity spectrum by the rapid distortion theory when the airfoil thickness is no longer negligible. Following this idea, Christophe [29] derived the exact modification of the von Kármán spectrum with the rapid distortion theory. This is also summarized in the review article by Roger and Moreau [37]. In the present work, the modified von Kármán isotropic model proposed by Ref. [29] is adopted to account for the airfoil leading-edge turbulence distortion phenomena

$$\Phi_{ww}(k_1, k_2) = \frac{91}{36\pi}\frac{u'^2}{k_e^2}\frac{k_1^2/k_e^2 + k_2^2/k_e^2}{\left(1 + k_1^2/k_e^2 + k_2^2/k_e^2\right)^{19/6}} \,. \tag{13}$$

Here, the important parameters to be obtained from experimental or numerical data are the turbulence integral length scale Λ, that should be measured away from the airfoil leading edge, and the velocity fluctuations u', which should be measured in the proximity of the leading edge. Further details about this model are presented by de Santana *et al.* [26].

Results

In this section, we present results obtained by the proposed numerical technique. For all figures in this section, the term "FP" represents solutions obtained for a flat plate, the term "Fin" relates to results computed using Amiet's formulation for a finite span theory, "Inf" represents solutions computed using Amiet's formulation with the infinite span assumption and "InvS" relates to solutions obtained by the inverse strip theory. Some observations provided in this section are discussed in Ref. [38] and, here, we include additional results for the effect of leading-edge bluntness on the acoustic radiation.

Model validation

For validation purposes, we combine the modifications described in this paper for Amiet's theory and apply the resulting model for a jet-airfoil interaction noise problem. The results are then compared to those presented in Ref. [29]. Here, the problem consists of a NACA 0012 profile with $c = 2b = 0.041$ m chord and $2d = 8.78c$ span placed at zero angle of attack and at $6c$ distance from the jet outlet. The jet diameter and the airfoil chord have both the same length and the jet outlet velocity, U_0, is fixed at 13.2 m/s, resulting in a flow Reynolds number based on the airfoil chord length close to 36,000. A commercial software was used to simulate the unsteady turbulent flow around the airfoil and the far-field sound spectrum of the numerical simulation was obtained through Curle's formulation. The far-field measurements were performed at an observer distance of $4.878c$ from the airfoil center. In addition, an experiment was conducted under similar geometrical and flow conditions. The reader is referred to Ref. [29] for details about both the numerical and experimental procedures.

Figure 2 (b) presents the comparison of the noise spectra for the NACA 0012 profile using different approaches. Considering the functions obtained with the numerical simulation (Fig. 2 (a)), the spectrum from the combined model shows an excellent agreement with both experimental and numerical results, validating the present methodology. At frequencies above $\mathrm{He} \approx 3$, a mismatch between the the current numerical model and the other results is found, but this is expected. We observe in Fig. 2 that the high-frequencies are dominated by the background noise. Furthermore, LES simulations usually fail to represent high-frequency phenomena due to resolution/numerical dissipation issues.

Analysis of noise generation by spanwise-varying inflow conditions

In this section we assume a hypothetical flow with properties varying significantly along the span direction. This reproduces a scenario close to that encountered in rotating devices. The far-field noise predictions are then performed using the techniques described in this work. In this case, the mean flow, integral length scale and velocity fluctuation root-mean-square are assumed to have a linear variation along the span such that their respective minimum and maximum values occur at the span limits. The non-uniform mean flow velocity varies from 25 to 55 m/s, and the velocity fluctuation root-mean-square is given by $u'(y) = 0.06\,U(y)$, where $y \in [-d, d]$ represents the spanwise position. Finally,

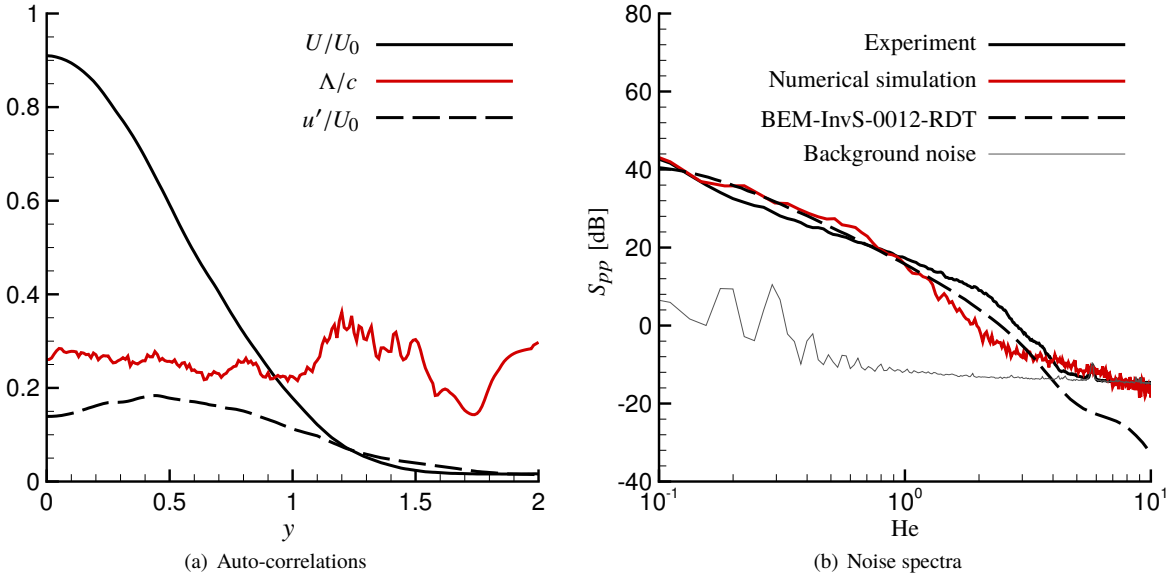

(a) Auto-correlations (b) Noise spectra

Fig. 2 Comparison of spectra obtained for a jet-airfoil noise interaction using a NACA 0012 profile.

the integral correlation length varies linearly from 0.0125 m to 0.0130 m. The magnitude of these values is based on the experimental work from Ref. [26].

Acoustic predictions are computed assuming either the previously described non-uniform inflow condition or a uniform inflow. When the uniform inflow is considered, the spanwise distribution is spatially averaged, i.e., the mean velocity is computed as $U_0 = 1/(2d)\int_{-d}^{+d} U(y)dy$. In the following results, the wing consists of a uniform section with $c = 2b = 0.1$ m chord and $2d = 1$ m span. Acoustic predictions are performed considering a far-field observer position $\mathbf{x} = (0, 0, R)$, with $R = 30c$. The center of the Cartesian system is positioned in the airfoil mid-chord and mid-span for the far-field noise computation.

Figure 3 (a) verifies the current implementation of the inverse strip method. In the present analysis, Amiet's formulation (Eq. 1) and the inverse strip technique should provide the same noise levels when one considers a high aspect ratio blade modeled as a flat plate subjected to uniform inflow conditions. This figure presents the acoustic pressure PSD considering three different formulations assuming uniform inflow conditions. Here, the inverse strip solution is compared to the results of Eq. 1 (infinite span formulation) and Eq. 11 (finite span formulation) where the black lines and symbols represent results of a blade of span $2d = 1$ m. In this test case, the three approaches lead to the same results in the whole frequency range, written in terms of the Helmholtz number $\mathrm{He} = kc$. To guarantee solution convergence and an affordable computational cost, the number of strips is set as $N_S = 20$ for the inverse strip method. The number of intervals of integration in Amiet's finite span formulation (Eq. 11) is $N_I = 800$.

For a low aspect ratio wing, the sine cardinal approximation adopted in the finite and infinite span calculations should lead to different results [25] . This case is also illustrated in Fig. 3 (a) where the acoustic prediction considers a short span flat plate with $2d = 0.2$ m (results shown in red color). In this figure, the legend titles are analogous to those from the black lines and symbols and, hence, they are omitted. The high-frequency content of the spectra are similar for the three methodologies analyzed. However, for low-frequencies, the infinite span assumption and the inverse strip method fail to reproduce the correct solution obtained by the "finite span" integration given by Eq. 11.

Figure 3 (b) compares the aeroacoustic transfer function solutions obtained analytically, prescribed by Amiet's theory [27] and by the BEM, both for a flat plate. Here, the flat plate aspect ratio is set as 10 ($2d = 1$ m). The infinite span assumption is expected to be a good approximation when the BEM calculation is applied since the finite span formulation would be computationally expensive. Furthermore, if such assumption is not satisfied, the evaluation of spanwise-varying inflow conditions would rely on the direct strip method through calculation of Eq. 11, what could be problematic as shown in Ref. [25] .

Figure 3 (b), verifies the convergence of the numerical method (BEM) by comparing results with the analytic solution for a flat plate. Note that the curves Inf-FP-VK in Fig. 3 (a) and (b) are the same. These analyses allow an

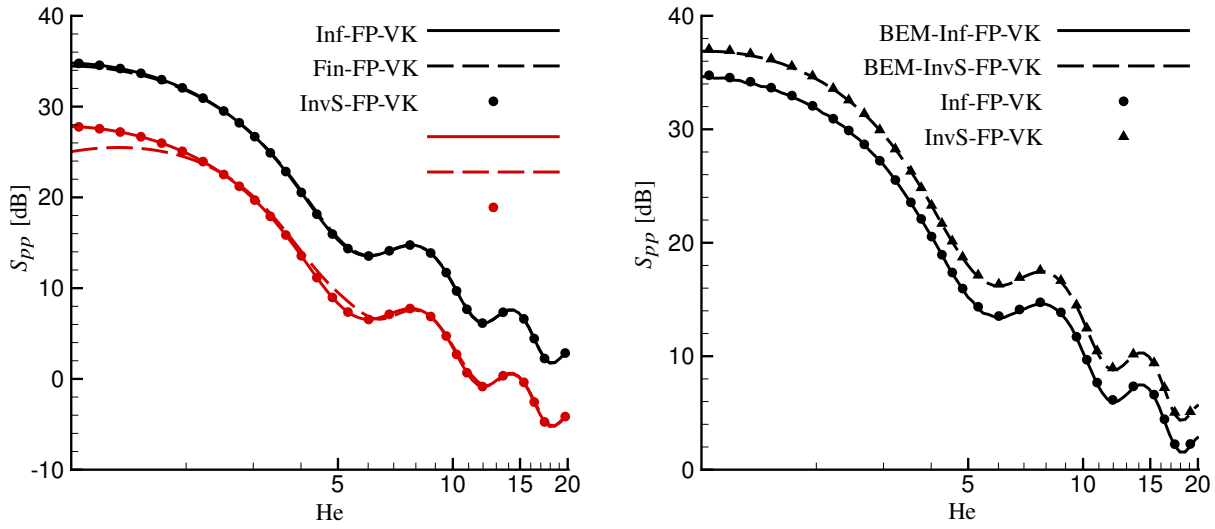

(a) Spanwise-uniform inflow conditions

(b) Spanwise-varying inflow conditions

Fig. 3 Acoustic spectra obtained for a flat plate and the von Kármán model for isotropic turbulence. Black and red legends indicate the long and short spans, $2d = 1.0$ and 0.2 m, respectively.

assessment of the effects of non-uniform spanwise inflow quantities through use of the inverse strip method and show that the BEM and infinite span solutions (Eq. 1) have an excellent agreement. The inverse strip solution, which accounts for non-uniform inflows, predicts increased noise levels when compared to the infinite span solution that considers a uniform inflow. For the current flow configuration, the predicted noise radiation increase is observed for all frequencies, reaching around 4 dB.

The numerical calculation of the gust-airfoil lift response requires the application of boundary conditions analogous to the Schwarzschild problem [24] . As shown in the previous reference, this procedure requires a computational domain extending from beyond the airfoil limits. Here, to assure that the low-frequencies are properly solved, two different domain limits are employed: $x_s \in [-7, 9]$ (using 5000 boundary elements) for frequencies higher than He = 5 and $x_s \in [-15, 17]$ (using 10000 boundary elements) for lower frequencies. The thickness of the extended computational domain is set to $t = 0.008b$ in the BEM calculation (see Ref. [24] for details). The numerical approach used here to compute the aeroacoustic transfer function performs two iterations of the analogous Schwarzschild problem, including the leading-edge scattering and the trailing-edge backscattering. Such approach shows good results for moderate and high-frequencies, however, the method presents discrepancies for low Helmholtz numbers, He $\lesssim 1$, especially for oblique gusts [39]. In this previous case, more iterations of the Schwarzschild problem should be conducted.

As mentioned in Secs. A and D, when non-zero thickness airfoils are considered, the flow anisotropy and the reduction in the magnitude of the aeroacoustic transfer function may significantly contribute to the far-field noise prediction. Figure 4 shows how these effects alter the acoustic pressure PSD whether analyzed independently or combined. Figure 4 (a) presents results for a uniform inflow where the aeroacoustic transfer functions are obtained by the analytic solution for a flat plate, indicated by the solid lines. The aeroacoustic transfer functions are also computed for a NACA 0012 airfoil via the BEM solution, presented in dashed lines. For both cases, the von Kármán isotropic model (VK) and the modified model through rapid distortion theory (RDT) are assessed in the predictions. Figure 4 (b) shows similar results, however, considering a non-uniform inflow.

For the present flow configuration, the turbulence distortion occurs close to the airfoil leading-edge exhibiting the noise reduction expected by Glegg and Devenport [34] in the high-frequency range of the spectra. However, a notable increase in the noise radiation occurs at low-frequencies when the RDT is accounted for. The aeroacoustic transfer function, $\mathcal{L}$, obtained numerically for the NACA 0012 airfoil reduces the acoustic pressure PSD in a general sense, except for He $\simeq 6$, where the S_{pp} remains unaltered from that of the flat plate. However, this is merely due to the specific observer location. Finally, by comparing Figs. 4 (a) and (b), the uniform and spanwise-varying inflow conditions are compared showing an increase of the PSD levels of about 2 to 4 dB for the latter case.

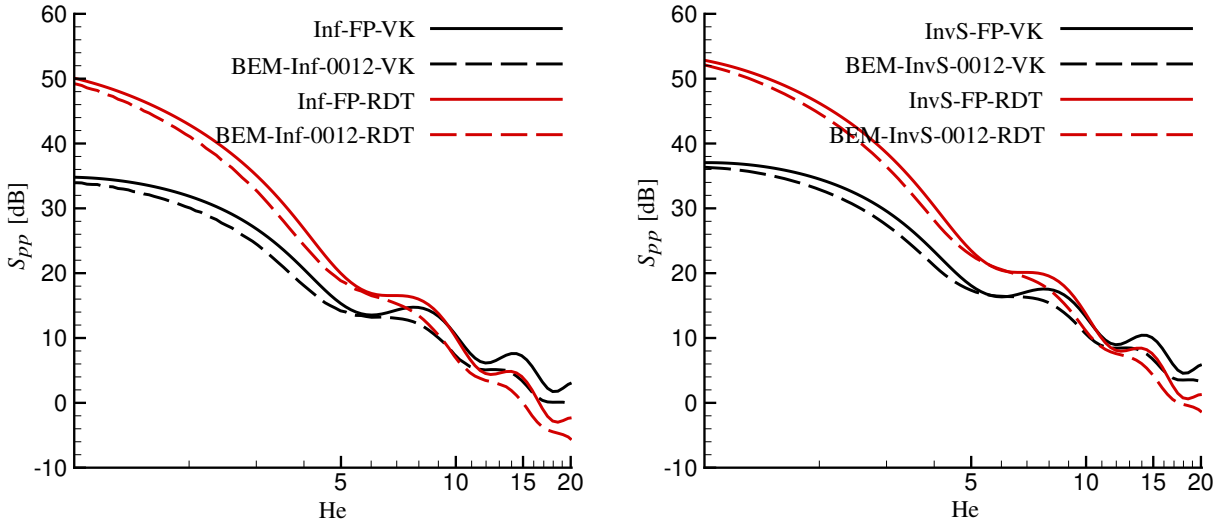

(a) Infinite span formulation (uniform inflow)

(b) Inverse strip method (non-uniform inflow)

Fig. 4 Spectra for a NACA 0012 profile comparing the influence of the von Kármán isotropic model (VK), the modified model through rapid distortion theory (RDT), and the modified aeroacoustic transfer function from the BEM.

Analysis of the airfoil thickness and the leading-edge geometry

Figure 6 shows results of the effects of airfoil thickness and local leading-edge geometry on gust-airfoil interaction noise. We compare the PSDs obtained by different aeroacoustic transfer functions computed for NACA profiles 0006, 0012 and 0018, and for modified NACA profiles 0012-03 and 0012-103[40]. Figure 5 illustrates the modified NACA 0012 airfoils. All transfer functions are computed by the proposed BEM approach. Moreover, we employ the same geometrical and inflow configurations from the work of Ayton and Chaitanya [6] for the noise prediction. Thus, the airfoil chord and span are set as $c = 2b = 0.15$ m and $2d = 0.45$ m respectively, and far-field measurements are performed at an observer distance of $R = 1.2$ m from the airfoil center. Here, we consider two different observer position being $\mathbf{x}^{(1)} = (0, 0, R)$ and $\mathbf{x}^{(2)} = (R\cos\theta, 0, R\sin\theta)$, with $\theta = 40$ deg based on the streamwise direction. The mean inflow velocity is 80 m/s ($M_0 = 0.24$) with a 2.5% turbulence intensity and a 7.5 mm integral length scale. The results in Fig. 6 assume isotropic turbulence, in accordance with Ref. [6].

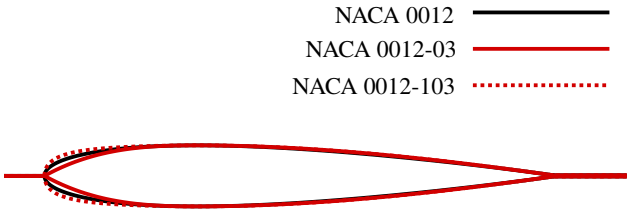

Fig. 5 Modified NACA 0012 airfoil profiles studied in this work. The lines extending from beyond the airfoil limits are a small portion of the computational domain required for the BEM solution, where the Kutta and Sommerfeld boundary conditions are applied.

For the observer location $\mathbf{x}^{(1)}$ (Fig. 6 (a)), the modified NACA 0012-03 is found to have the highest levels of noise over the entire spectral range when compared against the other profiles analyzed. At high-frequencies, we observe a reduction of the spectral levels of more than 2 dB between the NACA 00120-03 and the NACA0012-103 (or NACA0018). These results show that the shape of the leading edge can be as important for the noise radiation as the overall thickness of the airfoil profile. For example, for this observer position, the noise from the NACA 0006 airfoil has lower PSD levels than those from the NACA 00120-03 configuration for high Helmholtz numbers.

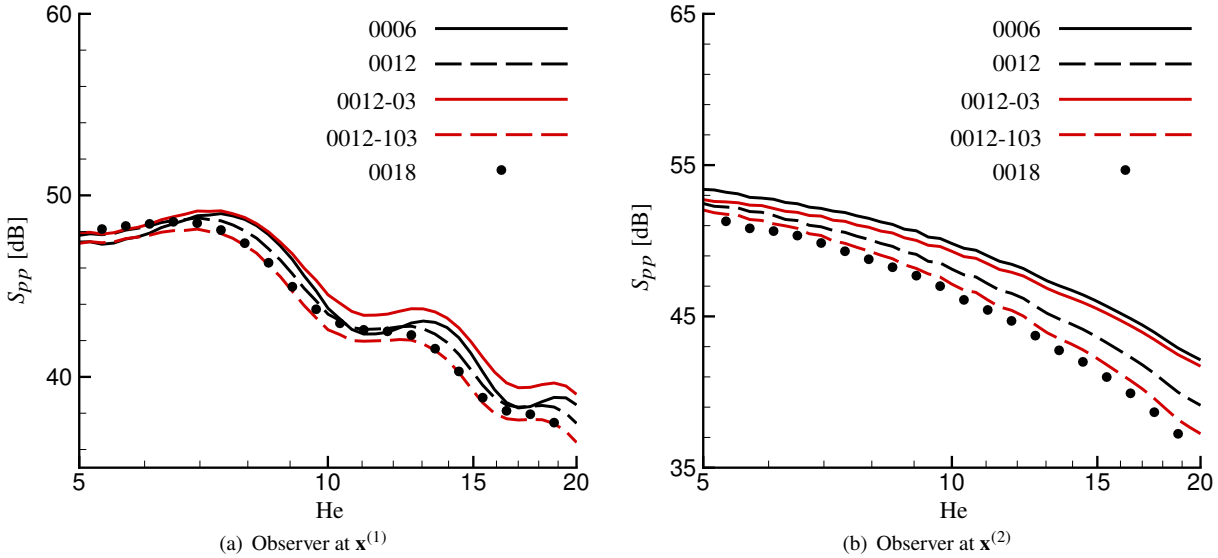

(a) Observer at $\mathbf{x}^{(1)}$ (b) Observer at $\mathbf{x}^{(2)}$

Fig. 6 Comparison of spectra obtained for a NACA 0006, NACA 0012, NACA 0012-03, NACA 0012-103 and a NACA 0018 profile using the von Kármán model for isotropic turbulence. All aeroacoustic transfer functions are computed using the BEM.

A second observer location at $\mathbf{x}^{(2)}$ is considered in Fig. 6 (b). This observer is placed at a 40 deg. angle with respect to the streamwise direction, corresponding to a region of the scattered acoustic field where more pronounced lobes appear in the pressure directivities for the higher Helmholtz numbers analyzed. In this case, the aeroacoustic transfer function has a higher impact in the noise prediction, especially at high-frequencies, where the differences between the S_{pp} levels are found to be up to 6 dB. Previous work [6, 24, 28, 35, 36] show that, for high frequencies and thick airfoil profiles, the directivities change from the typical cardioid shape to that of a compact dipole source. Hence, for downstream angles, one should expect a noise reduction for thick profiles. The same effect is observed for blunt leading edges.

From both Figs. 6 (a) and (b), we observe that modifying the leading-edge radius has a similar effect of modifying the airfoil overall thickness. As one can see, the spectrum of a NACA 0012-03 is very close to that of a NACA 0006. In the same context, the spectrum of the NACA 0012-103 is similar to that of the NACA 0018. These results show the same trends found in the literature [6, 41–43].

Conclusions

This work investigates the contribution from different methodologies employed together with Amiet's theory for the leading-edge noise prediction. The current methodology allows the noise prediction of general airfoil profiles with spanwise-varying inflow conditions. We combine the inverse strip method for non-uniform inflows with the rapid distortion theory, RDT, to calculate the two-dimensional turbulence spectrum and the boundary element method, BEM, to compute the aeroacoustic transfer function of general airfoil profiles.

It is shown that the RDT plays the most significant role on far-field noise prediction. For high frequencies, when the airfoil can be regarded as a non-compact source, the RDT model leads to a reduction in the radiated far-field noise when compared to the von Kármán model for isotropic turbulence. A similar observation is found in the literature. However, for the low-frequency range, noise levels are considerably increased with the RDT model. The spanwise-varying inflow conditions analyzed in the current work are found to raise the pressure PSD from 2 to 4 dB compared to the uniform inflow case investigated. On the other hand, the airfoil-gust lift response computed for an airfoil with finite thickness is shown to reduce the noise levels, especially for observer positions downstream of the airfoil and for higher frequencies. Results also show that a blunter leading edge generates an analogous effect similar to that of increasing the airfoil thickness, *i.e.*, the reduction of the far-field noise.

Acknowledgements

The authors gratefully acknowledge the support for this research provided by Fundação de Amparo à Pesquisa do Estado de São Paulo, FAPESP, under Research Grants No. 2013/03413-4 and No. 2013/07375-0, and by Conselho Nacional de Desenvolvimento Científico e Tecnológico, CNPq, under Research Grant No. 305277/2015-4. The computational resources provided by Centro Nacional de Processamento de Alto Desempenho, CENAPAD-SP, under Project 551, are also gratefully acknowledged. The authors also acknowledge FAPESP for providing MSc. and PhD. scholarships to the first author under Grants No. 2015/19538-6 and 2017/10795-1, respectively. Finally, the 4TU Research Centre Fluid & Solid Mechanics (FSM) is acknowledged for a one month working visit of Mr. Miotto and Dr. Wolf to the Netherlands during which part of this work was done. The authors gratefully acknowledge Dr. Julien Christophe for providing the data used in Fig. 2.

References

[1] Glegg, S., Baxter, S., and Glendinning, A., "The prediction of broadband noise from wind turbines," *Journal of Sound and Vibration*, Vol. 118, No. 2, 1987, pp. 217–239.

[2] Blandeau, V. P., Joseph, P. F., Jenkins, G., and Powles, C. J., "Comparison of sound power radiation from isolated airfoils and cascades in a turbulent flow," *The Journal of the Acoustical Society of America*, Vol. 129, No. 6, 2011, pp. 3521–3530.

[3] Kim, J. W., Haeri, S., and Joseph, P. F., "On the reduction of aerofoil–turbulence interaction noise associated with wavy leading edges," *Journal of Fluid Mechanics*, Vol. 792, 2016, pp. 526–552.

[4] Giez, J., Roger, M., Vion, L., and Moreau, S., AIAA AIATION Forum, American Institute of Aeronautics and Astronautics, 2017, Chaps. Effects of Intermittency and Geometry on the Turbulence Impingement Noise of a CROR Rear-Rotor Blade. doi:10.2514/6.2017-3217, 0.

[5] Quaglia, M., Leonard, T., Moreau, S., and Roger, M., "A 3D analytical model for orthogonal blade-vortex interaction noise," *Journal of Sound and Vibration*, Vol. 399, 2017, pp. 104–123.

[6] Ayton, L. J., and Chaitanya, P., "Analytical and experimental investigation into the effects of leading-edge radius on gust–aerofoil interaction noise," *Journal of Fluid Mechanics*, Vol. 829, 2017, p. 780–808. doi:10.1017/jfm.2017.594.

[7] Narayanan, S., Chaitanya, P., Haeri, S., Joseph, P., Kim, J. W., and Polacsek, C., "Airfoil noise reductions through leading edge serrations," *Physics of Fluids*, Vol. 27, No. 2, 2015, p. 025109. doi:10.1063/1.4907798.

[8] Gea Aguilera, F., Gill, J. R., Angland, D., and Zhang, X., AIAA AVIATION Forum, American Institute of Aeronautics and Astronautics, 2017, Chap. Wavy Leading Edge Airfoils Interacting with Anisotropic Turbulence. doi:10.2514/6.2017-3370, 0.

[9] Chaitanya, P., Joseph, P., Narayanan, S., Vanderwel, C., Turner, J., Kim, J. W., and Ganapathisubramani, B., "Performance and mechanism of sinusoidal leading edge serrations for the reduction of turbulence–aerofoil interaction noise," *Journal of Fluid Mechanics*, Vol. 818, 2017, p. 435–464. doi:10.1017/jfm.2017.141.

[10] Roger, M., Schram, C., and De Santana, L., "Reduction of Airfoil Turbulence-Impingement Noise by Means of Leading-Edge Serrations and/or Porous Material," , 2013. doi:10.2514/6.2013-2108.

[11] Amiet, R., "Acoustic radiation from an airfoil in a turbulent stream," *Journal of Sound and Vibration*, Vol. 41, No. 4, 1975, pp. 407 – 420.

[12] Curle, N., "The influence of solid boundaries upon aerodynamic sound," *Proceedings of the Royal Society of London. Series A, Mathematical and Physical Sciences*, Vol. 231, No. 1187, 1955, pp. pp. 505–514.

[13] Howe, M. S., "On unsteady surface forces, and sound produced by the normal chopping of a rectilinear vortex," *Journal of Fluid Mechanics*, Vol. 206, 1989, p. 131–153. doi:10.1017/S0022112089002259.

[14] Küssner, H. G., "Zusammenfassender Bericht über den istationären Auftrieb von Flügeln," *Luftfahrtforch*, , No. 12, 1936, pp. 410 – 424.

[15] Sears, W. R., "Some aspects of non-stationary airfoil theory and its practical application," *Journal of the Aeronautical Sciences*, Vol. 8, No. 3, 1941, pp. 104–108.

[16] Goldstein, M. E., and Atassi, H., "A complete second-order theory for the unsteady flow about an airfoil due to a periodic gust," *Journal of Fluid Mechanics*, Vol. 74, No. 04, 1976, pp. 741–765.

[17] Atassi, H., "The Sears problem for a lifting airfoil revisited-new results," *Journal of Fluid Mechanics*, Vol. 141, 1984, pp. 109–122.

[18] Howe, M., "Unsteady lift and sound produced by an airfoil in a turbulent boundary layer," *Journal of Fluids and Structures*, Vol. 15, No. 2, 2001, pp. 207–225.

[19] Ayton, L. J., and Peake, N., "On high-frequency sound generated by gust–aerofoil interaction in shear flow," *Journal of Fluid Mechanics*, Vol. 766, 2015, pp. 297–325.

[20] Gennaretti, M., Luceri, L., and Morino, L., "A unified boundary integral methodology for aerodynamics and aeroacoustics of rotors," *Journal of Sound and Vibration*, Vol. 200, No. 4, 1997, pp. 467 – 489.

[21] Zhou, Q., and Joseph, P., "A frequency domain numerical method for airfoil broadband self-noise prediction," *Journal of Sound and Vibration*, Vol. 3, 2007, pp. 504–519.

[22] Gennaretti, M., Testa, C., and Bernardini, G., "An unsteady aerodynamic formulation for efficient rotor tonal noise prediction," *Journal of Sound and Vibration*, Vol. 332, 2013, pp. 6743–6754.

[23] Glegg, S. A., and Devenport, W. J., "Panel methods for airfoils in turbulent flow," *Journal of Sound and Vibration*, Vol. 329, No. 18, 2010, pp. 3709 – 3720.

[24] Miotto, R. F., Wolf, W. R., and Santana, L. D., "Numerical computation of aeroacoustic transfer functions for realistic airfoils," *Journal of Sound and Vibration*, Vol. 407, 2017, pp. 253–270.

[25] Christophe, J., Anthoine, J., and Moreau, S., "Amiet's theory in spanwise-varying flow conditions," *AIAA Journal*, Vol. 47, No. 3, 2009, pp. 788 – 790.

[26] de Santana, L. D., Christophe, J., Schram, C., and Desmet, W., "A rapid distortion theory modified turbulence spectra for semi-analytical airfoil noise prediction," *Journal of Sound and Vibration*, Vol. 383, 2016, pp. 349 – 363.

[27] Amiet, R. K., "High frequency thin-airfoil theory for subsonic flow," *AIAA Journal*, Vol. 14, No. 8, 1976, pp. 1076–1082.

[28] Paterson, R. W., and Amiet, R. K., "Noise and surface pressure response of an airfoil to incident turbulence," *Journal of Aircraft*, Vol. 14, No. 8, 1977, pp. 729–736.

[29] Christophe, J., "Application of hybrid methods to high frequency aeroacoustics," Ph.D. thesis, von Karman Institute for Fluid Dynamics, 2011.

[30] Rozenberg, Y., Roger, M., Guédel, A., and Moreau, S., Aeroacoustics Conferences, American Institute of Aeronautics and Astronautics, 2007, Chap. Rotating Blade Self Noise: Experimental Validation of Analytical Models. doi:10.2514/6.2007-3709, 0.

[31] Batchelor, G. K., and Proudman, I., "The effect of rapid distortion of a fluid in turbulent motion," *The Quarterly Journal of Mechanics and Applied Mathematics*, Vol. 7, No. 1, 1954, pp. 83–103. doi:10.1093/qjmam/7.1.83.

[32] Hunt, J. C. R., "A theory of turbulent flow round two-dimensional bluff bodies," *Journal of Fluid Mechanics*, Vol. 61, 1973, pp. 625 – 706.

[33] Migliore, P., and Oerlemans, S., "Wind tunnel aeroacoustic tests of six airfoils for use on small wind turbines," Tech. Rep. NREL/CP-500-35090, National Renewable Energy Laboratory, 2003.

[34] Glegg, S. A., and Devenport, W., "Unsteady loading on an airfoil of arbitrary thickness," *Journal of Sound and Vibration*, Vol. 319, No. 3-5, 2009, pp. 1252 – 1270.

[35] Lockard, D. P., and Morris, P. J., "Radiated Noise from Airfoils in Realistic Mean Flows," *AIAA Journal*, Vol. 36, No. 6, 1998, pp. 907–914. doi:10.2514/2.494.

[36] Moreau, S., Roger, M., and Jurdic, V., "Effect of Angle of Attack and Airfoil Shape on Turbulence-Interaction Noise," 11^{th} *AIAA/CEAS Aeroacoustics Conference (*26^{th} *AIAA Aeroacoustics Conference)*, 2005.

[37] Roger, M., and Moreau, S., "Extensions and limitations of analytical airfoil broadband noise models," *International Journal of Aeroacoustics*, Vol. 9, No. 3, 2010, pp. 273–305. doi:10.1260/1475-472X.9.3.273.

[38] Miotto, R. F., Wolf, W. R., and de Santana, L. D., "Leading-edge noise prediction of general airfoil profiles with spanwise-varying inflow conditions," *AIAA Journal*, Vol. 56, No. 5, 2018, pp. 1711–1716. doi:10.2514/1.J056716.

[39] Miotto, R. F., Wolf, W. R., and de Santana, L. D., "Numerical computation of airfoil-gust lift response with applications to leading-edge noise generation," *AIAA Paper 2017-3693, 23^{rd} AIAA/CEAS Aeroacoustics Conference*, 2017.

[40] Ladson, C. L., Brooks Jr., C. W., Hill, A. S., and Sproles, D. W., "Computer program to obtain ordinates for NACA airfoils," Tech. Rep. NASA 4741, National Advisory Committee for Aeronautics, December 1996.

[41] Devenport, W. J., Staubs, J. K., and Glegg, S. A., "Sound radiation from real airfoils in turbulence," *Journal of Sound and Vibration*, Vol. 329, No. 17, 2010, pp. 3470 – 3483.

[42] Hall, A., Atassi, O., Gilson, J., and Reba, R., "Effects of leading-edge thickness on high-speed airfoil-turbulence interaction noise," *17th AIAA/CEAS Aeroacoustics Conference, Portland, Oregon, AAIA Pap*, Vol. 2861, 2011, p. 2011.

[43] Gill, J., Zhang, X., and Joseph, P., "Symmetric airfoil geometry effects on leading edge noise," *The Journal of the Acoustical Society of America*, Vol. 134, No. 4, 2013, pp. 2669–2680.